CRYSTAL GROWTH & DESIGN

Article

pubs.acs.org/crystal

Crystallographic Control in the Replacement of Calcite by Calcium Sulfates

Encarnacion Ruiz-Agudo,*[,†] Pedro Álvarez-Lloret,[‡] Aurelia Ibañez-Velasco,[†] and Miguel Ortega-Huertas[†]

[†]Department of Mineralogy and Petrology, University of Granada, Fuentenueva s/n, 18002 Granada, Spain

[‡]Department of Geology, University of Oviedo, c/Jesús Arias de Velasco, s/n, 33005, Oviedo, Spain

ABSTRACT: The transformation of calcite into calcium sulfate phases in the presence of an aqueous phase is relevant to many technological processes, including remediation of acid mine drainage, exploitation of subsurface reservoirs, geological CO_2 sequestration, and the conservation of building stone. At acidic pH, the interaction of sulfate-bearing aqueous solutions with calcite cleavage fragments results in the replacement of gypsum, bassanite, and/or anhydrite depending on the reaction time and temperature. Here we show that a fraction of the calcium sulfate crystals (gypsum, bassanite, or anhydrite) grows in all cases oriented onto the calcite surfaces, forming a product layer that reproduces the initial morphology of the calcite crystals. Calcium sulfates form on calcite surfaces as thick three-dimensional crystals, suggesting a Volmer−Weber mechanism of epitactic growth. The epitaxial relationships found by two-dimensional X-ray diffraction are $(010)_{Gp}//(104)_{Cal}$; $(010)_{Bs}//(104)_{Cal}$; and $(200)_{Anh}//(104)_{Cal}$ and are discussed on the basis of the structure of calcite and the different sulfate phases. Apparently, sulfate phases form in all cases with their crystallographic *c*-axis parallel to the <$\bar{4}$41> periodic bond chain (PBC) of calcite. Ca−Ca repeating periods in $CaSO_4$ phases along the <001> direction range from 6.336 to 6.491 Å, thus closely matching that of <$\bar{4}$41> PBC of calcite (6.425 Å).

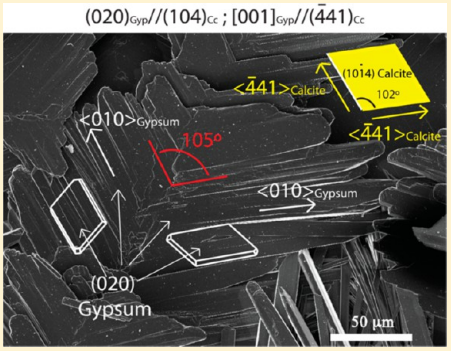

INTRODUCTION

Mineral replacement reactions involving carbonate and sulfate phases have important geological and industrial implications. In particular, the replacement of calcite ($CaCO_3$) by calcium sulfates (gypsum, $CaSO_4{\cdot}2H_2O$, bassanite, $CaSO_4{\cdot}0.5H_2O$ and anhydrite, $CaSO_4$) is relevant to issues as varied as exploitation of subsurface carbonate rocks as oil, gas and groundwater reservoirs,[1] geological CO_2 sequestration,[2] the preservation of stone-built cultural heritage,[3−5] remediation of sulfate-bearing acid mine drainage (AMD), flue gas desulfurization at high temperatures, and cement production.[6] In these systems, the replacement of precursor carbonate minerals by sulfates can significantly modify the porosity and pore size distribution of the original mineral assemblage. These properties are critical in most of the applications described above. For example, the characteristics of the pore system can potentially affect many technical and industrial aspects related to the effective exploitation of carbonate rocks as hydrocarbon reservoirs[7] or CO_2 repositories. As well, the formation of gypsum upon calcite dissolution during AMD treatment makes it ineffective once the newly formed precipitates completely cover the original substrate and consequently protect the surface from further reactions.

During replacement reactions, the generation of porosity will be ultimately determined by molar volume and relative solubility differences between the parent and product phases, the formation of fractures, and/or the presence of grain boundaries, as well as the existence or not of epitaxy and the type of growth mechanism of the product phase.[8] The relevance of the structural matching between parent and product phases in a replacement reaction for the development of porosity and the progress of the reaction has been shown, for example, in the case of the replacement of calcite and aragonite by a $(Cd,Ca)CO_3$ solid solution.[9] The existence of a high structural matching between this solid solution and the calcite substrate results in the formation of a compact, nanometer-thick layer of oriented $(Cd,Ca)CO_3$ crystallites, which isolates the substrate from further dissolution, so that the replacement process stops. However, in the case of aragonite, growth of thick three-dimensional (3D) $(Cd,Ca)CO_3$ crystals on the aragonite surface takes place as the degree of crystallographic matching is lower. In this latter case, the surface does not become passivated by the reaction product as pathways for the fluid to reach the unreacted aragonite are formed in the contact between nonaligned product crystals.[9]

Previous experimental studies have suggested some kind of structural or crystallographic control during $CaCO_3$−$CaSO_4$ transformation. For example, the lattice matching between calcite and the overgrowing gypsum has been claimed to promote a strong adhesion between both phases, thus making gypsum the main phase responsible for calcite surface passivation during AMD treatment.[4,10] As well, there is strong evidence that the gypsum layer formed during sulfation of carbonate building stones (marbles, limestones, and dolo-

Received: April 6, 2016
Revised: June 29, 2016
Published: July 26, 2016

DOI: 10.1021/acs.cgd.6b00522
Cryst. Growth Des. 2016, 16, 4950−4959

stones) in urban environments is pseudomorphic with the original calcite substrate and preserves the original details of the stone, and, therefore, it should be conserved when conservation treatments are applied.[11] Moreover, oriented nucleation and growth of anhydrite onto calcite surfaces during direct sulfation of limestone at high temperature have been reported based on scanning electron microscopy (SEM) observations of reacted calcite surfaces.[6] Both calcite and calcium sulfate phases are common components of scales which forms in a range of technological applications.[12] The formation of the mixed scales may be quite usual, and some mixed deposits may require an epitactic relationship to be formed.[13] In this regard, the formation of barite- and calcite-calcium sulfate mixed scales has been suggested as a method to reduce scale formation or as a way to control crystal morphology.[14−16]

However, despite the importance of the type of (epitactic) growth mechanism in determining the control of the $CaCO_3$ to $CaSO_4$ transformation and the porosity developed, as well as in the overgrowth of calcium sulfate phases onto calcite, to our knowledge such aspects remain essentially unexplored. This study aims at filling this gap in knowledge, and it is part of a broader study that deals with such transformations, with the ultimate goal of improving our understanding of the mechanisms ruling the replacement reactions involving carbonates and sulfates and the factors determining the porosity development during such processes. In this work, we have focused on the crystallographic features of the conversion of calcite into calcium sulfate at different temperatures. To determine the 3D crystallographic relationship between $CaCO_3$ to $CaSO_4$ we have analyzed the orientation of the parent calcite crystal and the product(s) in partially transformed crystals using X-ray diffraction texture analysis. This technique allows us to obtain several pole figures containing detailed information about the specific orientation of the crystals that make up polycrystalline materials.[17] This information, together with an analysis of the crystalline structures of parent and product phases, can give us important insights into crystallographic control and the distribution of volume and porosity in the replacement product during this transformation.

MATERIALS AND METHODS

Replacement Reactions in Teflon Reactors. Cleavage fragments (0.030 ± 0.005 mg weight, ca. 4 × 3 × 1 mm in size) of optical quality calcite single crystals (Iceland spar) were reacted with 100 mM H_2SO_4 solutions (pH 1.10). These conditions were selected in order to speed up the reactions and to observe the replacement process at a laboratory timeline. The experiments were conducted in tetrafluoroethylene-lined steel autoclaves (3 mL inner volume) held at room temperature (20 ± 2 °C) and in an oven at 60, 120, and 200 ± 1 °C for 1 to 288 h. The solubility of the relevant Ca-sulfate phases (gypsum, bassanite and anhydrite) at these temperatures (llnl database) is given in Table 1. For each experiment 1.5 mL of solution was added to the autoclave containing the crystal fragments that was then sealed and weighed. In the experiments performed at T > 20 °C, the oven was preheated to the required temperature before the autoclaves were placed inside. The samples were weighed at the end of the experiment after being cooled in air to ensure that no fluid had been lost. After the experiments the crystals were removed from the solution, washed with ethanol, and dried. A JEOL 6300F field emission scanning electron microscope (FESEM) equipped with a backscattered electron (BSE) and energy-dispersive X-ray (EDX) detector was used for morphology and texture examinations. The observations were carried out at an accelerating voltage of 3 kV.

Two-Dimensional X-ray Diffraction Analysis of Reacted Solids. Two-dimensional (2D) X-ray diffraction and pole figures describing the 3D orientation of the calcite (Iceland spar fragments) and calcium sulfate mineral phases were determined using an X-ray single crystal diffractometer equipped with a CCD area detector (D8 SMART APEX, Bruker, Germany). The working conditions for the diffraction experiments were Mo Kα (λ = 0.7093 Å), 50 kV, and 30 mA. The diffraction patterns were registered by reflection mode setting the ω and 2θ diffractometer angles at 10° and 20°, respectively. A set of 2D diffraction patterns were registered while rotating the sample around the Φ angle (a frame was registered every 5°) with a pinhole collimator of 0.5 mm in diameter, and an exposure time of 20 s per frame. The corresponding pole figures represent the 3D distribution of the poles of (hkl) crystallographic planes associated with each hkl diffraction reflection analyzed.[18] Pole figures were calculated using XRD2DScan software.[17] The epitaxial relationships found and the theoretical morphology (i.e., that given by the prominence of each form derived from the unit cell and space group using the Donnay−Harker morphological law) of the different calcium sulfate phases was modeled using the SHAPE software.

Table 1. Solubility Product (log K_{sp}) of Gypsum, Bassanite, and Anhydrite As a Function of Reaction Temperature (°C) (llnl database)

	reaction temperature (°C)			
	25	60	120	200
anhydrite	−4.35	−4.78	−5.68	−7.29
gypsum	−4.53	−4.63	−5.05	−6.14
bassanite	−3.71	−4.13	−5.02	−6.6

RESULTS

Reaction Pathway of the $CaCO_3$−$CaSO_4$ Replacement. Calcite (Iceland spar) fragments were partially replaced by different calcium sulfates (gypsum, $CaSO_4{\cdot}2H_2O$, bassanite, $CaSO_4{\cdot}0.5H_2O$, and anhydrite, $CaSO_4$) depending on the reaction temperature. The external morphology is preserved during the replacement reaction; i.e., pseudomorphs are formed (Figure 1). After an interaction period of just 1 h, $CaSO_4$ phases grow on calcite surfaces mostly as bulk, thick micron-sized crystals with different morphologies depending on the reaction temperature (Figures 2, 3, and 4). The mineralogy of the phases precipitated under the different experimental conditions is summarized in Table 2. At room temperature,

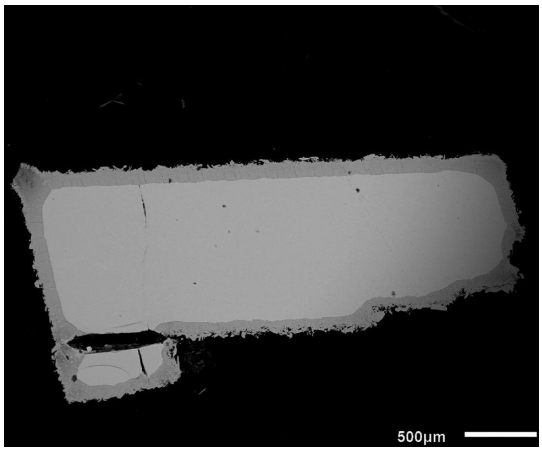

Figure 1. SEM backscattered electron image of a partially replaced calcite crystal in a 0.1 M H_2SO_4 solution at 60 °C during 12 days. Note the slightly darker, polycrystalline rim surrounding the inner calcitic core.

DOI: 10.1021/acs.cgd.6b00522
Cryst. Growth Des. 2016, 16, 4950−4959

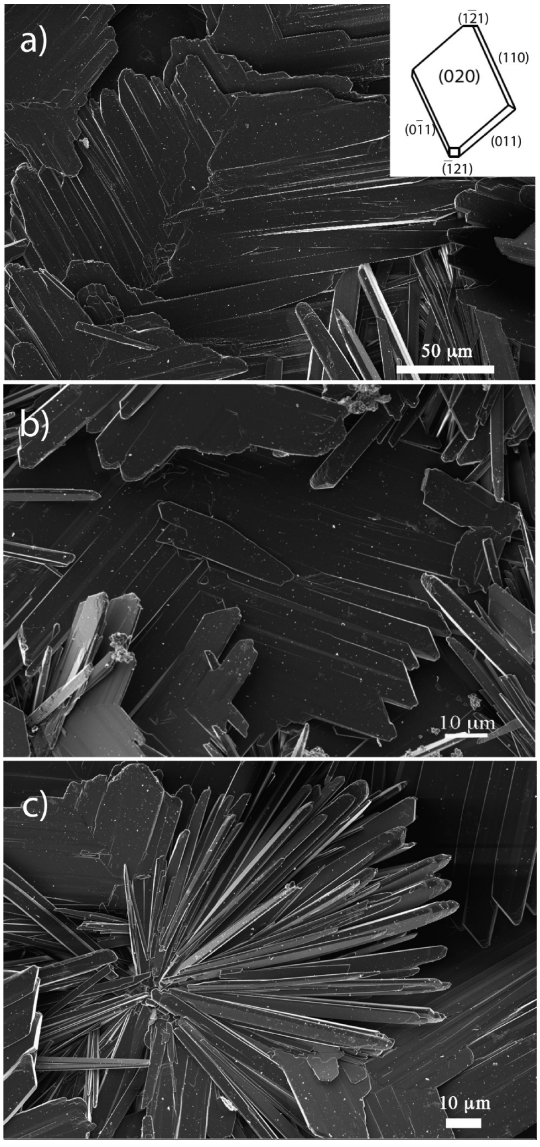

Figure 2. FESEM secondary electron images of gypsum crystals formed on calcite surfaces upon contact with sulfate bearing solutions (0.1 M H_2SO_4 solution at 25 °C). Together with thick, prismatic oriented crystals (a, b) radial aggregates of apparently unoriented crystals (c) are observed on the surface. Interaction time: (a–c) 120 h. The inset in (a) shows the theoretical morphology for gypsum calculated using SHAPE software.

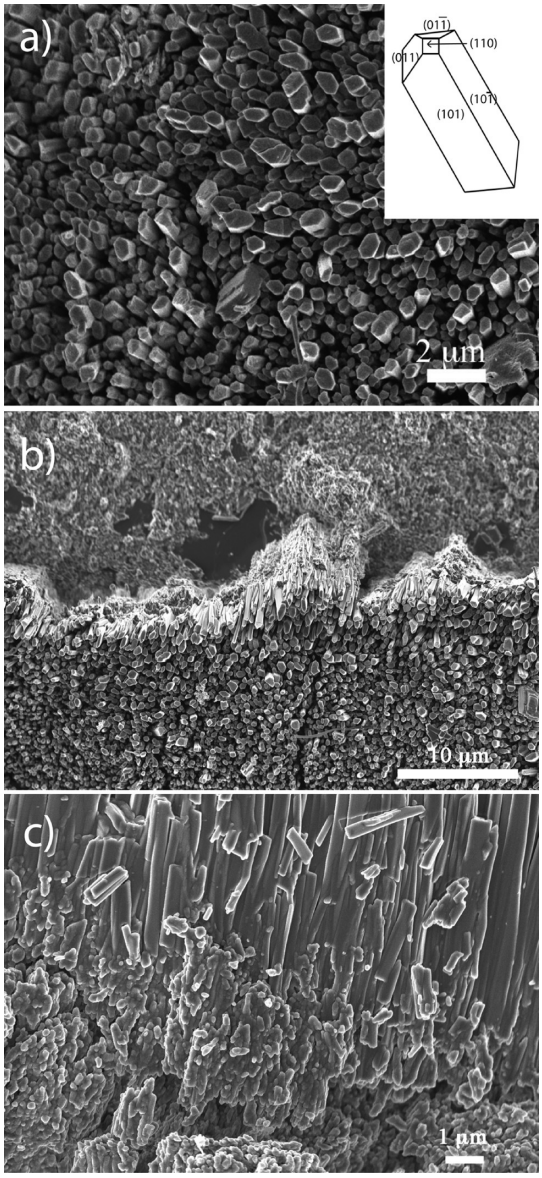

Figure 3. FESEM secondary electron images of oriented columnar bassanite crystals formed on calcite surfaces upon contact with sulfate bearing solutions (0.1 M H_2SO_4 solution at 120 °C). Interaction time: (a–c) 120 h. The inset in (a) shows the theoretical morphology for bassanite calculated using SHAPE software.

gypsum as the major phase (together with calcite) and trace amounts of bassanite were found at all reaction times; interestingly, bassanite was not detected previously at this temperature by GIAXRD.[12] The same applies for T = 60 °C. Part of the gypsum crystals formed at room temperature and 60 °C, identified by morphological criteria and in agreement with two-dimensional X-ray diffraction (2D-XRD) results, appear twinned with the two individuals in the twin oriented on the calcite substrate along two directions related by an angle of ca. 105°, very similar to that of the obtuse corner of the calcite rhombohedra −102° (Figure 2a,b). Bassanite could not be unambiguously identified on the surface of crystals replaced at room temperature and 60 °C. At 120 °C, 2D-XRD analysis shows the coexistence of gypsum and bassanite in the reaction rim after 1 h of reaction, bassanite and anhydrite at t = 24 h and only anhydrite at $t \geq 120$ h. 2D-XRD analyses of samples reacted at 200 °C show the presence of both bassanite and anhydrite at t = 1 h, and the presence of anhydrite as the only Ca-sulfate phase for $t \geq 24$ h. Apparently, bassanite seems to form initially as nanoparticles that aggregate into nanorods, which subsequently attach in an oriented manner to give larger crystals (Figure 3). Through this sequence of oriented aggregation steps, the final bassanite crystals would appear oriented with respect to the calcite substrate surface, in a similar way as it is seen in Figure 3. Subsequently, elongated planar crystals growing in all cases outward from the calcite surface, with different rotation angles, are observed (Figure 4a,b). These crystals could be anhydrite, or more likely partially transformed bassanite; the square or rectangular islands observed could be anhydrite forming on the precursor bassanite (Figure 4c). Finally, after 12 days of interaction, bulk planar anhydrite crystals appear randomly distributed on the calcite surface; apparently, anhydrite seems to lose its initial orientation with

DOI: 10.1021/acs.cgd.6b00522
Cryst. Growth Des. 2016, 16, 4950–4959

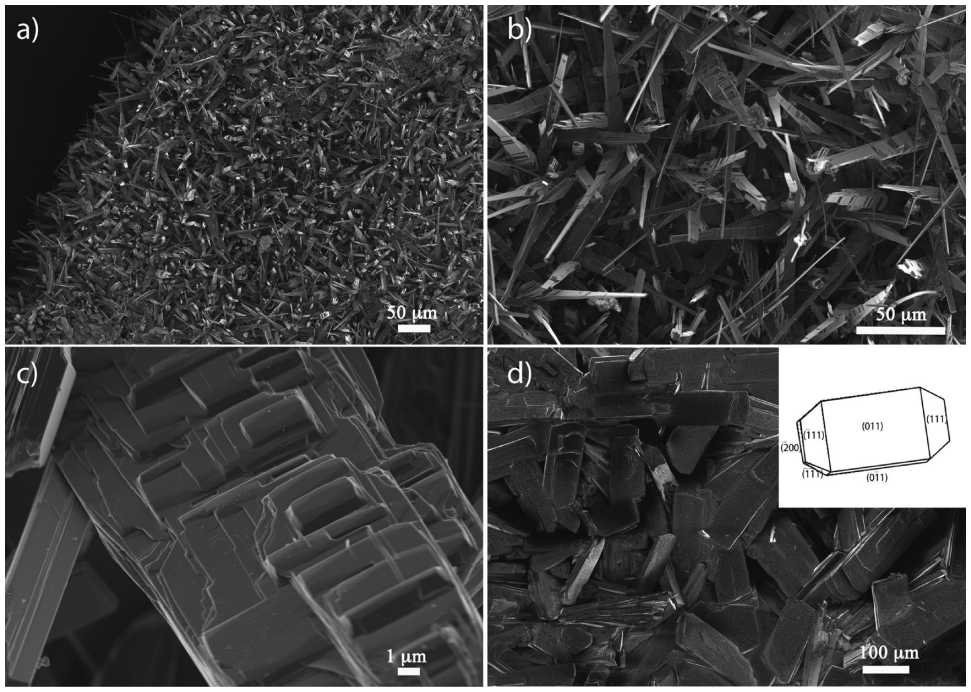

Figure 4. FESEM secondary electron images of calcium sulfate crystals (bassanite and anhydrite) formed on calcite surfaces upon contact with sulfate bearing solutions (0.1 M H_2SO_4 solution at 200 °C). Crystals show acicular to tabular morphologies, particularly in the early stages of the precipitation reaction. Interaction time: (a) 24 h, (b) 24 h, (c) 120 h, and (d) 288 h. The inset in (d) shows the theoretical morphology for anhydrite calculated using SHAPE software.

Table 2. Mineralogical Evolution during the $CaCO_3$ to $CaSO_4$ Transformation, As a Function of Reaction Temperature (°C) and Time (h)

reaction temperature (°C)	reaction time (h)			
	1	24	120	288
25	gypsum bassanite	gypsum bassanite	gypsum bassanite	gypsum bassanite
60	gypsum bassanite	gypsum bassanite	gypsum bassanite	gypsum bassanite
120	gypsum bassanite	gypsum anhydrite	anhydrite	anhydrite
200	anhydrite bassanite	anhydrite	anhydrite	anhydrite

respect to the calcite substrate, possibly inherited from the precursor bassanite (Figure 4d). Further details of the microscopic features of replacement textures and evolution of the chemistry of the solutions are reported elsewhere,[12] while this study deals exclusively with the growth mechanism and the crystallographic control existing between calcite and calcium sulfates during the replacement process.

Analysis of Crystallographic Preferred Orientations of $CaSO_4$ Phases. In the calcium sulfate system, gypsum is monoclinic (space group $I2/a$, a_0 = 5.679 Å, b_0 = 15.202 Å, and c_0 = 6.522; β = 118.43; Hildyard et al. 2011 refs therein),[19] whereas the crystal structure of bassanite is described as either trigonal, or monoclinic but pseudotrigonal. Here we use the $I2$ setting (a_0 = 12.032 Å, b_0 = 6.927 Å, and c_0 = 12.671; β = 90.27) to describe bassanite structure.[19] Anhydrite crystallizes in the orthorhombic system,[19] space group *Amma*, with lattice parameters a_0 = 6.993 Å, b_0 = 6.995 Å, and c_0 = 6.245 Å. In these settings, the Ca−SO_4−Ca chains in the three calcium sulfate phases are oriented in the direction of the *c*-axis. Calcite crystallizes in the trigonal system (space group $R\bar{3}c$), with the calcium cations and carbonate groups occupying alternate layers perpendicular to the *c* axis.

The analysis of the 2D X-ray diffraction patterns of samples partially replaced by gypsum (room temperature and 60 °C) shows the presence of strong/well-defined diffraction spots from the calcite crystal (cleavage surface) and several diffraction Debye−Scherrer rings of the gypsum crystals (Figure 5a). Superimposed on these diffraction rings (corresponding to *hkl* reflections) the intensity is concentrated in arcs, which indicates that a fraction of the gypsum crystals have a preferential orientation. The preferential orientation of the gypsum crystals in relation to the calcite cleavage surface was further characterized by the determination of pole figures for the main and secondary (*hkl*) reflections of both mineral phases obtained from the unidimensional diffraction pattern (Figure 5b). The pole figure for the (012) reflection of calcite indicates that the sample is oriented on the plane of the cleavage surface (Figure 5c). The pole figure for the (020) reflection of overgrowth gypsum crystals shows a maximum (showing some degree of dispersion) at the center of the pole figure (Figure 5d) that coincides with the orientation of (104) calcite cleavage surface (i.e., pole figure center). On the other hand, the pole figure for the gypsum ($12\bar{1}$) reflection (not shown) displays two shaded maximum tilted by approximately 55° with respect to the pole figure center, which coincides with the (020) reflection for gypsum. Thus, our 2D-XRD analyses indicate that gypsum grows epitactically on calcite, with $(010)_{Gyp}//(104)_{Cc}$. This orientation relationship of gypsum onto calcite may have been inherited from that of bassanite (see below), which is apparently a precursor phase to gypsum precipitation at these lower temperatures, and transferred possibly during the dissolution−precipitation transformation of bassanite into gypsum.[12] A simulation of the epitactic relationship found in

DOI: 10.1021/acs.cgd.6b00522
Cryst. Growth Des. 2016, 16, 4950−4959

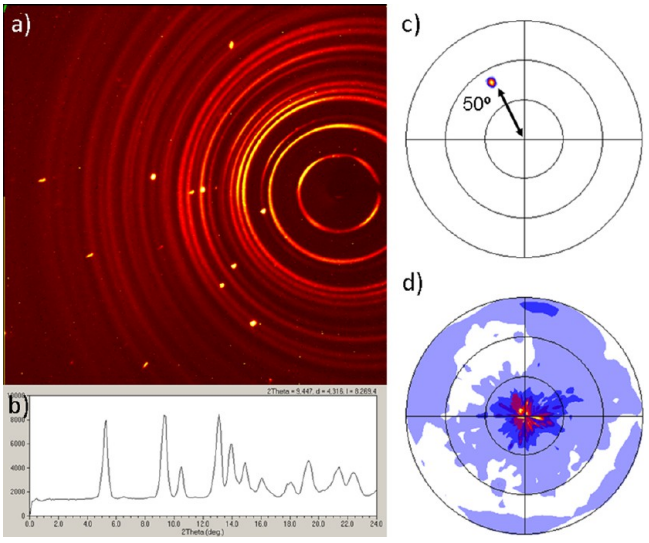

Figure 5. (a) Two-dimensional X-ray diffraction (2D-XRD) pattern (phi-rotation scan) of calcite crystals partially replaced by gypsum at 25 °C. Strong single diffraction spots belong to the parent calcite (cleavage surface), while Debye−Scherrer rings correspond to gypsum crystals. The fact that intensities are concentrated in arcs within the Debye−Scherrer rings indicates a preferred crystal orientation of part of the gypsum crystals. (b) 2θ scan profile obtained from the radial integration of the 2D-XRD pattern. (c) 012 calcite pole figure showing a maximum tilted ca. 50° with respect to the center of the pole figure, indicating that the sample is oriented in the 104 cleavage plane. (d) 020 pole figure for gypsum showing a maximum at the center, indicating that gypsum forms with its (010) plane parallel to (104) plane of calcite.

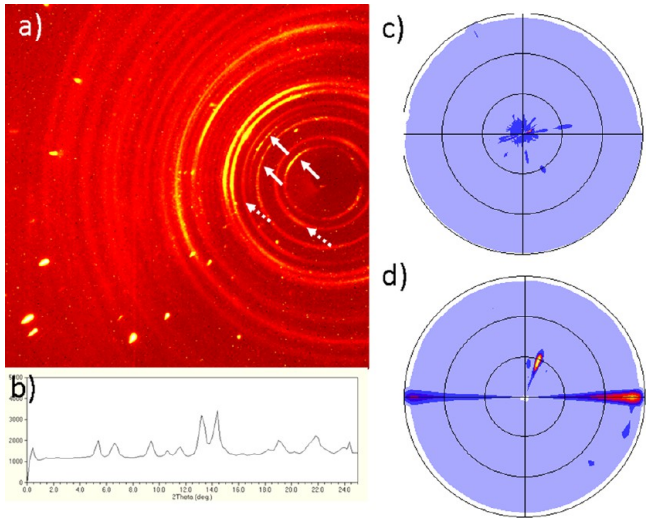

Figure 6. (a) Two-dimensional X-ray diffraction (2D-XRD) patterns (phi-rotation scan) from calcite crystals partially replaced by gypsum and basanite at 120 °C (1 h). Strong single diffraction spots belong to the parent calcite, while Debye−Scherrer rings correspond to gypsum (solid arrow line) and bassanite (dotted arrow line) crystals. (b) 2θ scan profile obtained from the radial integration of the 2D-XRD pattern. (c) 020 pole figure for bassanite showing a maximum at the center of the pole figure, indicating that the sample is co-oriented in the 104 calcite cleavage plane. (d) 200 pole figure for bassanite showing two maxima tilted ca. 90° and a maximum for 110 bassanite tilted ca. 30° from the center of the figure, indicating that bassanite forms (020) coincides with the center of the figure.

this study is shown in Figure 9. The epitaxy can be characterized by considering the matching between the two structures along the [001] direction of gypsum and the [$\bar{4}$41] direction of calcite (Figure 10). The misfit among these directions is calculated as in Rodriguez-Blanco et al.[20] or Ruiz-Agudo et al.:[21,22]

$$\text{mf}\,(\%) = \frac{2(t_{[uvw]\text{Cal}} - t_{[uvw]\text{CS}})}{t_{[uvw]\text{Cal}} + t_{[uvw]\text{CS}}}$$

where $t_{[uvw]}$ is the Ca−Ca repeating period along the [uvw] direction in calcite (Cal) and calcium sulfate phases (CS). For gypsum, $t_{[001]}$ is 6.491 Å, and for calcite, $t_{[-441]}$ is 6.425 Å. This means a misfit of about −1.0%, which is within the limits required for epitactic nucleation from solution. Additionally, a good matching was found between the cell vectors 3x[0$\bar{1}$0] + 2x[$\bar{4}$12] in calcite (17.019 Å) and 3x[100] in gypsum (16.860 Å) (misfit ca. 0.9%). Matching directions in calcite are related by an angle of 112.5°, while in the case of gypsum the corresponding angle is 118.5° (i.e., the angular misfit between these matching directions is ca. 6°).

Similar analyses were performed for calcite samples partially replaced at 120 °C during 1 h (Figure 6). Under these conditions, bassanite and gypsum coexist in the replacement rim. At this temperature, gypsum and bassanite have similar solubility and are both metastable with respect to anhydrite and should have probability similar to precipitate. Apparently, under this condition gypsum is the first phase to form, and further replacement toward the core of the calcite substrate continues in the form of bassanite.[12] Gypsum crystals showed the same orientation relationship with respect to calcite than that found at 25 and 60 °C. Interestingly, our results show that a fraction of the bassanite crystals forms as well with a preferred orientation on calcite cleavage surfaces. The pole figure for the (020) reflection of overgrowth bassanite crystals shows a maximum (low diffraction intensities) at the center of the pole figure, which coincides with the (104) calcite cleavage surface (Figure 6c). Additionally, the pole figure of the (200) reflection of bassanite shows two maxima tilted by approximately 90° and a maximum for (110) reflection tilted ca. 30° from the center of the pole figure that coincides, as previously pointed out, with the (020) reflection of bassanite crystals (Figure 6d). This orientation relationship confirms that the parent calcite and precipitated bassanite crystals show the following crystallographic relationship: $(104)_{\text{Cal}}\|(010)_{\text{Bs}}$. A simulation of this epitactic relationship is shown in Figure 9. In this case, the misfit between the calcite and bassanite structures along the [001] direction of bassanite (6.336 Å) and the [$\bar{4}$41] direction of calcite (6.425 Å) was found to be 1.4%, which is within the limits required for epitactic nucleation from solution. In this case, simultaneous matching along other directions on $(010)_{\text{Bs}}$ and $(104)_{\text{Cal}}$ planes was not found.

Finally, the analysis of the 2D-XRD patterns of calcite samples partially replaced by anhydrite at T = 120 °C ($t \geq 24$ h) shows as well that the diffraction intensity in the observed Debye−Scherrer rims is concentrated in arcs, and thus a fraction of the anhydrite crystals have a preferential orientation (Figure 7a). Analysis of the pole figure for the (200) reflection of anhydrite crystals in the replacement rim shows a maximum located at the center of the figure (Figure 7c) that coincides with the orientation of (104) calcite cleavage surface (pole figure not shown). This is further confirmed by the pole figure for the anhydrite (202) reflection, which displays two shaded

DOI: 10.1021/acs.cgd.6b00522
Cryst. Growth Des. 2016, 16, 4950−4959

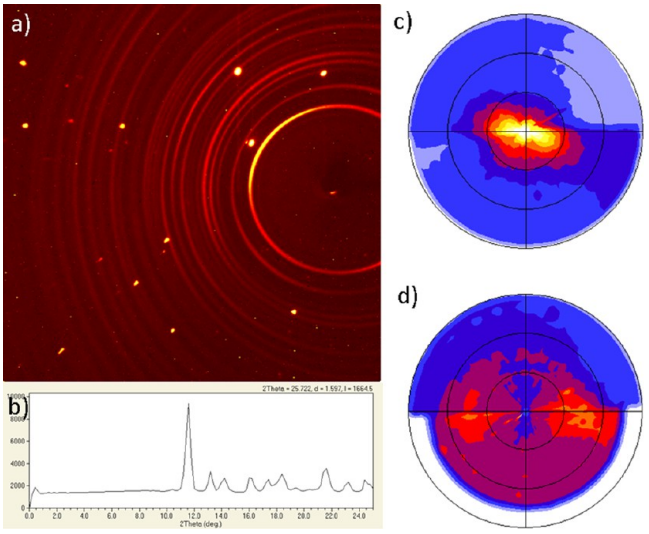

Figure 7. (a) Two-dimensional X-ray diffraction (2D-XRD) patterns (phi-rotation scan) from calcite crystals partially replaced by anhydrite at 120 °C (24 h). (b) 2θ scan profile obtained from the radial integration of the 2D-XRD pattern. (c) 200 pole figure for anhydrite showing a maxima at the center of the figure, indicating that the sample is oriented in the 104 cleavage plane (pole figure not shown). (d) 202 pole figure for anhydrite showing two shaded maximum tilted ca. 48° from the center of the figure, coinciding with the 200 pole figure for anhydrite.

maximum tilted by approximately 45° with respect to the pole figure center that coincides with the (200) reflection for anhydrite (Figure 7d). These two maximum are equivalent as are related to the anhydrite {202} crystal form, tilted by approximately 96° between them. From these analyses of the pole figures (PF) obtained from 2D-XRD patterns, we conclude that the following crystallographic orientation relationship exists between calcite cleavage surface and replacing anhydrite crystals: $(200)_{Anh}//(104)_{Cal}$. Following a similar approach to that of gypsum and bassanite, a misfit of 2.8% is found between the [001] direction of anhydrite (6.245 Å) and the [$\bar{4}$41] direction of calcite (6.425 Å). Again, this orientation relationship of anhydrite onto calcite may have been inherited from that of bassanite (see above), which is apparently a precursor phase to anhydrite precipitation at this temperature and transferred possibly during the dissolution–precipitation transformation of bassanite into anhydrite. The misfit found is still within the limits for epitactic growth. Additionally, a good matching was found between the cell vectors 3x[0$\bar{1}$0] + 2x[$\bar{4}$12] in calcite (17.019 Å) and 2x[001] + 5x[011] in anhydrite (17.764 Å) (misfit ca. −4.3%). Matching directions in calcite are related by an angle of 112.5°, while in the case of anhydrite the corresponding angle is 100.1° (i.e., the angular misfit between these matching directions is ca. −12°). Similar orientation relationships were found for bassanite and anhydrite formed at 200 °C (t = 1 h), although crystals show a lower degree of preferential orientation. At reaction times >1 h at 200 °C, bassanite crystals were not presented, and anhydrite progressively increased its crystal size as preferential orientation practically disappeared. Figure 8 shows as with reaction times the anhydrite crystals peak intensities increased in the bidimensional X-ray diffraction pattern as well as the number of crystals illuminated by X-ray beam decreased and so did the number of reflection. This methodology was extensively described elsewhere.[18]

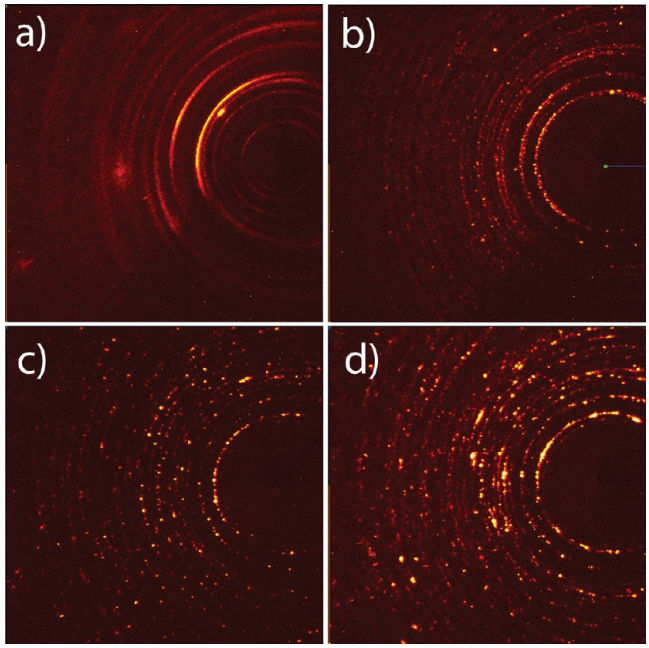

Figure 8. Crystal size and preferential orientation evolution of anhydrite crystals at 200 °C on calcite cleavage surface. Two-dimensional X-ray diffraction patterns of partially replaced crystals upon contact with sulfate solutions during (a) 1 h, (b) 24 h, (c) 120 h, (d) 12 days.

DISCUSSION

The reaction of Island spar crystals with a H_2SO_4 solution produces pseudomorphs made of different $CaSO_4$ phases, depending on the temperature conditions and reaction time, which accurately reproduce the external morphology of the original calcite crystal surface. Previous studies suggest that this occurs most likely via an interface-coupled dissolution–precipitation reaction, in which the substrate is replaced pseudomorphically by the product.[10,12] The mineralogical evolution of calcium sulfate phases formed during the $CaCO_3$–$CaSO_4$ transformation characterized here by means of 2D-XRD analyses is, in general, in agreement with GIAXRD results reported by Ruiz-Agudo et al.[12] Nevertheless, trace amounts of bassanite were observed at 25 and 60 °C in this study at all reaction times, which were not detected in our previous work.[12] At 120 °C, gypsum and bassanite coexist in the replacement rim after 1 h of reaction, and a small amount of anhydrite was detected after 24 h, which was also not detected previously using GIAXRD. Our results confirm that bassanite appears as a precursor phase to gypsum (25 and 60 °C) and anhydrite (120 and 200 °C), at least in the initial stages of the reaction. Nevertheless, direct precipitation of anhydrite cannot be ruled out exclusively from our observations. Interestingly, bassanite crystals grow from nanoparticles via different steps of oriented aggregation, following a growth mechanism very similar to that proposed by Van Driessche and co-workers[23] for the homogeneous nucleation and growth of gypsum via the formation of bassanite as a precursor.

Our previous work on this system pointed to a strong structural control on the $CaCO_3$ to $CaSO_4$ transformation. Indeed, 2D-XRD results presented here indicate a clear crystallographically preferred orientation of the three Ca-SO_4 phases formed during the interaction of calcite with sulfate bearing solutions, directed by the crystal structure of the calcite

DOI: 10.1021/acs.cgd.6b00522
Cryst. Growth Des. 2016, 16, 4950–4959

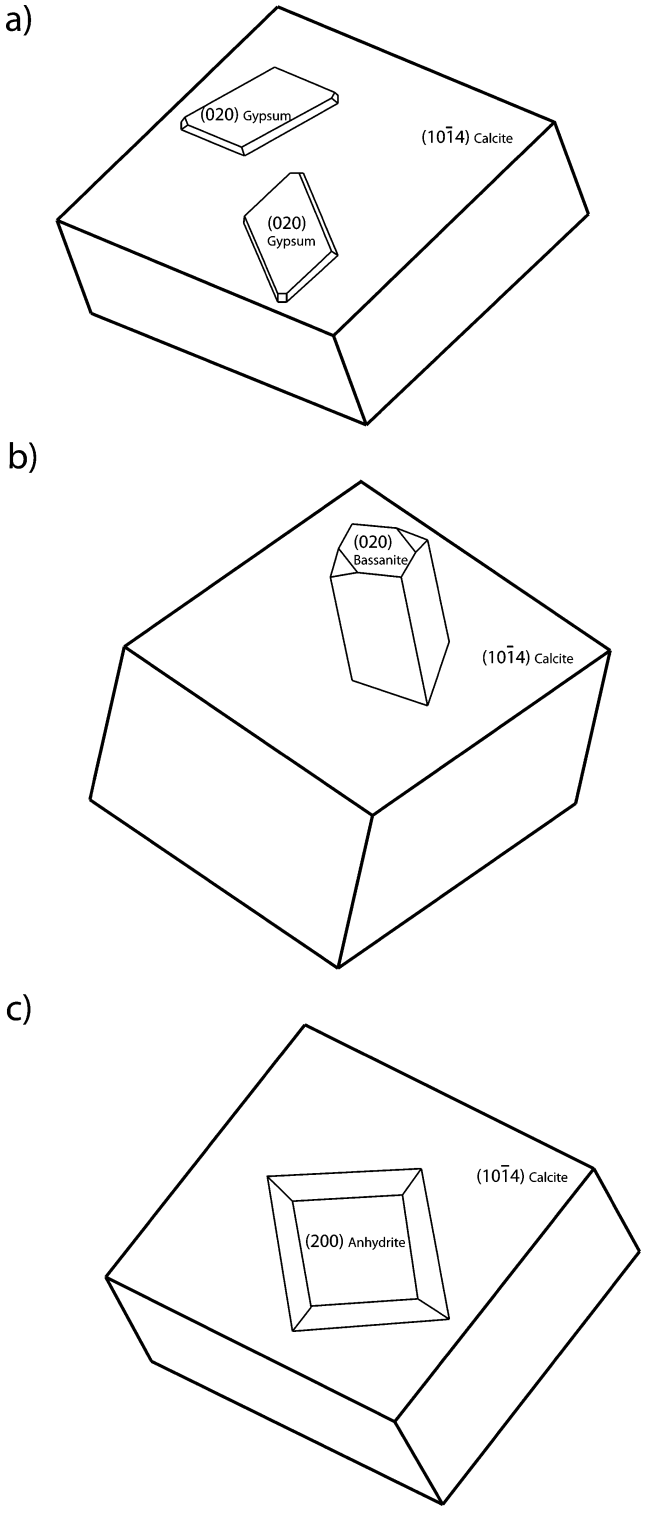

Figure 9. Model for epitaxial relationships between calcium sulfate and calcite phases: (a) gypsum, bassanite, and anhydrite crystals nucleate epitaxially with their (a) {0001}, (b) {0001}, and (c) {001} planes parallel to {10.4} calcite surfaces, respectively.

substrate or inherited through subsequent transformations within $CaSO_4$ phases. This observation can be understood by comparison of the crystal structures of the relevant phases taking part in the system. Common structural motifs in all $CaSO_4$ phases are the Ca-SO_4 periodic bond chains (PBCs), where sulfate tetrahedra are coordinated through oxygen atoms with two neighboring Ca ions in the chain direction. In the three phases, Ca-SO_4 chains run parallel to the [001] direction. Similarly, in the {10$\bar{1}$4} calcite cleavage plane, the <$\bar{4}$41> PBC is formed by Ca-CO_3 chains. Our results suggest that the epitactic growth of calcium sulfates on calcite crystals is controlled by the very similar Ca−Ca distance in the strong PBCs running along the matching crystallographic directions in calcite (⟨$\bar{4}$41⟩) and gypsum, bassanite and anhydrite (⟨001⟩). The distances between calcium ions along these directions are 6.425 Å, for calcite crystal, and 6.491, 6.336, and 6.245 Å, for gypsum, bassanite, and anhydrite, respectively. In particular, we find the following epitactic relationships:

$$(104)_{Cal} \| (010)_{Gp}$$

$$(104)_{Cal} \| (010)_{Bs}$$

$$(104)_{Cal} \| (200)_{Anh}$$

The epitactic relationships observed between the parent calcite crystal and the different $CaSO_4$ crystalline forms during phase transformation reaction indicate that the mineral replacement must occur at the solution/mineral interface by the nucleation of $CaSO_4$ on the dissolving cleavage surface of calcite crystals. Moreover, subsequent mineral replacement of a specific $CaSO_4$ phase by another must also occur at the interface crystal solution, so that the orientation of the parent calcite determines the disposition of the crystals of the final $CaSO_4$ phase during transformation. The exact mechanism by which the crystallographic information is transferred in dissolution−precipitation reactions is not well understood yet. It has been suggested that upon contact of crystalline materials with aqueous solutions, an electrostatic field develops that influences the distribution of the surrounding water molecules, inducing a periodic water structure at the mineral surface at the nanometer scale.[24] These structures have been detected by force modulation atomic force microscopy[25] and predicted by molecular simulations.[26] The internal structure of crystalline materials is direction specific, and thus the intensity of the field in the direction perpendicular to nonequivalent surfaces could be significantly different. As for oriented aggregation of nanoparticles, when a new phase forms in the vicinity of a mineral surface, the interaction of fields emanating from both phases should result in a final interaction potential that is also direction-specific. The anisotropic gradient of the interaction energy should then drive the newly formed particle to co-orient with the substrate. In other words, water structuring at mineral−fluid interfaces might be a key player in interface-coupled dissolution−precipitation reactions, acting as a bridge for the transmission of crystallographic information among parent and product phases (via a moving fluid reaction interface).

However, despite the good matching found along specific directions of calcite and gypsum, bassanite and anhydrite, the angular misfit existing between matching directions in these structures could explain the fact that gypsum and anhydrite crystals grows as thick 3D crystals (Figures 2 and 4), instead of forming continuous layers or thin platelets morphologies on the calcite surface. These observations point toward a Volmer−Weber mechanism of epitactic growth, which is characteristic of weak adhesion between substrate and overgrowth. This would be in agreement with nanoscopic observations on a similar system[10] showing that sulfate phases grow as thick, oriented crystals on calcite and dolomite cleavage surfaces upon contact

DOI: 10.1021/acs.cgd.6b00522
Cryst. Growth Des. 2016, 16, 4950−4959

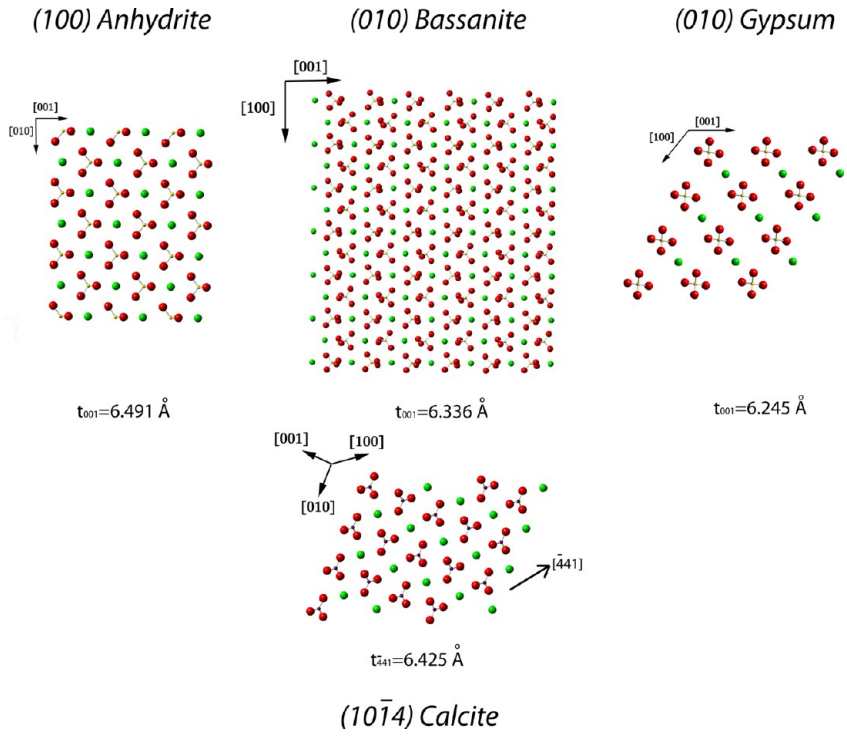

Figure 10. Crystal structure of the main planes of calcium sulfate and calcite phases. Note the correspondence between the periodic bond chains running along [001] in the different calcium sulfate phases and <$\bar{4}$41> in calcite, which have a similar distance between calcium ions.

with sulfate-bearing solutions. In the case of bassanite, there is also the issue that it does not seem to grow following a "classical" growth mechanism, but rather following particle-mediated growth mechanism. Nevertheless, if a good 2D matching between the substrate and the product phase would exist, growth by formation and spreading of nanometer-thick layers could be still expected but at the nanoscale, as it has been shown of the case of ACC growth on calcite[27] (Rodriguez-Navarro et al. 2016).

It is worth noting that the newly formed gypsum crystals can be oriented either with [001] parallel either to [$\bar{4}$41] or [48$\bar{1}$] directions of calcite related by an angle of 101.9°. This orientation corresponds to that of two classic gypsum twin laws, where the re-entrant angle is near 105°[28] (Rubbo et al. 2012). This phenomenon becomes evident in Figure 2. Thus, gypsum can grow onto the calcite cleavage surface with two alternative, statistically equivalent, orientations related by a *c*-glide, this resulting in the formation of twins. In other words, the twin law reproduced the symmetry axis present in the calcite substrate. In the image, the gypsum crystals have the (010) surface exposed. This type of extensive induced twinning as a result of the symmetry between substrate and overgrowth has been observed previously in the gypsum−brushite system,[29,30] and it is another piece of evidence of the crystallographic control on gypsum formation during the $CaCO_3$−$CaSO_4$ transformation. Because of the elongated, needle-like morphology of bassanite crystals (Figure 3), it was not possibly to detect if induced twinning also occurs during the precipitation of bassanite.

Finally, we also observed a second population of calcium sulfate crystals with no apparent orientation relationship with the parent calcite crystal. This population of randomly oriented crystals could be the result of a secondary nucleation event within the bulk solution, far from the mineral surface, so that the structure of the parent solid cannot direct the orientation of the newly formed crystals. As well, the increased crystal size of the sulfate phases during the reaction can also modify their primitive orientation with respect to the calcite surface. This phenomenon is particularly evident in the case of anhydrite formation with increasing reaction time. In this case, anhydrite crystal size increased while the degree of preferential orientation decreased during the evolution of the reaction onto the calcite surface.

Under our experimental conditions, the $CaCO_3$−$CaSO_4$ transformation occurs with a positive volume change, as the combined result of both the differences in molar volumes (calcite, 36.9 cm^3 mol^{-1}; gypsum, 74.4 cm^3 mol^{-1}; bassanite, 53.8 cm^3 mol^{-1}; anhydrite, 46.1 cm^3 mol^{-1}) and relative solubility of the parent and product phases.[12] This ultimately should result in passivation of the unreacted substrate before calcite attains equilibrium with respect to the bulk solution. Although the relative solubility of minerals and molar volume changes are important factors in determining the pseudomorphic transformation of minerals, the growth mechanism of the product phase is also a key variable to be considered during the analysis of porosity generation in mineral replacement processes, as it determines the way that the volume of product is distributed on the reacting solid. If a good epitactic fit exists between the parent and product phases, the product will grow by a layer-by-layer mechanism, homogeneously covering the parent phase. In contrast, if the structure of the product differs significantly from that of the substrate, it will tend to precipitate by 3D heterogeneous nucleation, and some pore space may form at the interface between the parent phase and the product.[9,21] This would be the case of our system, where thick $CaSO_4$ crystals are observed to form on $CaCO_3$ surfaces. Thus, complete coverage and passivation of the calcite surface may not immediately occur upon contact of calcite surfaces with sulfate bearing solutions.

DOI: 10.1021/acs.cgd.6b00522
Cryst. Growth Des. 2016, 16, 4950−4959

CONCLUSIONS

Here we report one of the multiple examples in which a pseudomorphic, interface-coupled dissolution precipitation reaction is associated with a crystallographic control exerted by the parent mineral due to a match between the substrate and product crystal structures. Similar epitactic growth mechanisms have been described in the anglesite−anhydrite, brushite−gypsum, calcite−apatite, or the calcite−oxalate systems.[21,22,29−32] The results of this study show that the replacement of calcite by calcium sulfates (gypsum, bassanite, and/or anhydrite, depending on the reaction time and temperature) is pseudomorphic, the external shape of the rombohedral calcite fragments being preserved during the reaction. Part of the replacing sulfate crystals inherit their orientation from the parent crystal by the epitactic nucleation on cleavage calcite surfaces. Thus, there is a clear crystallographic control during the replacement of calcite by calcium sulfates. The fact that structural matching exists along specific directions of the calcite substrate and the precipitating phase can result in a lower supersaturation needed for the nucleation of the new $CaSO_4$ phase on the surface of the parent calcite crystal, compared to that needed for the precipitation of the same phase in the bulk solution. This evidence would imply that the formation of calcite scales could indeed potentially increase the probability of $CaSO_4$ scale formation. Also, the observation that (i) thick, 3D sulfate crystals form on the surface of the parent mineral and (ii) lattice matching between parent and product phases occurs specifically along one crystallographic direction ($\langle\bar{4}41\rangle$ of calcite and <001> of gypsum, bassanite, and anhydrite) suggests that a Volmer−Weber mechanism of epitactic growth may best describe the formation of calcium sulfate phases on calcite. This mechanism has implications in the volume distribution during the $CaCO_3$−$CaSO_4$ transformation and thus in the development of porosity. The formation of thick $CaSO_4$ crystals implies that complete coherent coverage of the calcite surface by a sulfate layer may not immediately occur after the contact of calcite with sulfate bearing solutions; moreover, some pore space may be maintained at the contact between $CaSO_4$ crystals, which would possibly constitute pathways for the fluid to reach the unreacted mineral.

AUTHOR INFORMATION

Corresponding Author

*Tel: +34 958 240473. Fax: +34 958 243368. E-mail: encaruiz@ugr.es.

Notes

The authors declare no competing financial interest.

ACKNOWLEDGMENTS

The authors acknowledge support from the Spanish Government (Grant MAT2012-37584-ERDF), the Junta de Andalucía (research group RNM-179 and Project P11-RNM-7550), and CO2-REACT (UE-13-ITN-CO2-REACT-317235). E.R.-A. also acknowledges the Spanish Ministry of Economy and Competitiveness for financial support through a Ramón y Cajal grant.

REFERENCES

(1) García-Rios, M.; Dávila, G.; Offeddu, F. G.; Soler, J. M.; Cama, J. Reactions during CO_2 geological sequestration: dissolution of calcite and dolomite coupled to gypsum precipitation. *Macla* **2011**, *15*, 93−94.

(2) Ahr, W. M. *Geology of Carbonate Reservoirs: The Identification, Description and Characterization of Hydrocarbon Reservoirs in Carbonate Rocks*; John Wiley & Sons, Inc: New York, 2008.

(3) Rodriguez-Navarro, C.; Doehne, E. Salt weathering: influence of evaporation rate, supersaturation and crystallization pattern. *Earth Surf. Processes Landforms* **1999**, *24*, 191−209.

(4) Booth, J.; Hong, Q.; Compton, R. G.; Prout, K.; Payne, R. M. Gypsum overgrowths passivate calcite to acid attack. *J. Colloid Interface Sci.* **1997**, *192*, 207−214.

(5) Del Monte, M.; Sabbioni, C. Gypsum crusts and fly ash particles on carbonate outcrops. *Arch. Meteorol., Geophys. Bioklimatol., Ser. B* **1984**, *35*, 105−111.

(6) Hu, G.; Dam-Johansen, K.; Wedel, S. Oriented Nucleation and Growth of Anhydrite during Direct Sulfation of Limestone. *Cryst. Growth Des.* **2008**, *8*, 1181−1185.

(7) Mazzullo, S. J.; Chillingarian, G. V. Diagenesis and origin of porosity. In *Carbonate Reservoir Characterization: A Geologic Engineering Analysis*; Elsevier Publishing Company: Amsterdam. Mazzullo, S. J.; Chillingarian, G. V. *Dev. Pet. Sci.* 1992, *30*, 199−270, 10.1016/S0376-7361(09)70127-X.

(8) Ruiz-Agudo, E.; Putnis, C. V.; Putnis, A. Coupled dissolution and precipitation at mineral−fluid interfaces. *Chem. Geol.* **2014**, *383*, 132−146.

(9) Prieto, M.; Cubillas, P.; Fernandez-Gonzalez, A. Uptake of dissolved Cd by biogenic and abiogenic aragonite: a comparison with sorption onto calcite. *Geochim. Cosmochim. Acta* **2003**, *67*, 3859−3869.

(10) Offeddu, F. G.; Cama, J.; Soler, J. M.; Putnis, C. V. Direct nanoscale observations of the coupled dissolution of calcite and dolomite and the precipitation of gypsum. *Beilstein J. Nanotechnol.* **2014**, *5*, 1245−1253.

(11) Vergés-Belmin, V. Pseudomorphism of gypsum after calcite, a new textural feature accounting for the marble sulphation mechanism. *Atmos. Environ.* **1994**, *28*, 295−304.

(12) Ruiz-Agudo, E.; Putnis, C. V.; Hövelmann, J.; Álvarez-Lloret, P.; Ibáñez-Velasco, A.; Putnis, A. Experimental study of the replacement of calcite by calcium sulphates. *Geochim. Cosmochim. Acta* **2015**, *156*, 75−93.

(13) Gill, J. S.; Nancollas, G. H. The growth of gypsum crystals on Barite and calcite. *Desalination* **1979**, *29*, 247−254.

(14) Standiford, S. W.; Sinek, I. R. Stop Scale in Sea Water Evaporators. *Chem. Eng. Prog.* **1961**, *57*, 58−63.

(15) Gainey, R. L.; Thorp, C. A.; Cadwallader, E. A. $CaSO_4$ seeding prevents $CaSO_4$ scale. *Ind. Eng. Chem.* **1963**, *55*, 39−43.

(16) Fröhner, K. R.; Panahandeh, H. An advanced seeding process in saline water conversion. *Desalination* **1975**, *16*, 261−269.

(17) Rodriguez-Navarro, A. B. Registering pole figures using an X-ray single-crystal diffractometer equipped with an area detector. *J. Appl. Crystallogr.* **2007**, *40*, 631−634.

(18) Rodriguez-Navarro, A. B. XRD2DScan: New software for polycrystalline materials characterization using two-dimensional X-ray diffraction. *J. Appl. Crystallogr.* **2006**, *39*, 905−909.

(19) Hildyard, R. C.; Llana-Fúnez, S.; Wheeler, J.; Faulkner, D. R.; Prior, D. J. Electron backscattered diffraction (EBSD) analysis of bassanite transformation textures and crystal structure produced from experimentally deformed and dehydrated gypsum. *J. Petrol.* **2011**, *52*, 839−856.

(20) Rodríguez-Blanco, J. D.; Jiménez, A.; Prieto, M. Oriented overgrowth of pharmacolite ($CaHAsO_4{\cdot}2H_2O$) on gypsum ($CaSO_4{\cdot}2H_2O$). *Cryst. Growth Des.* **2007**, *7*, 2756−2763.

(21) Ruiz-Agudo, E.; Alvarez-Lloret, P.; Putnis, C. V.; Rodriguez-Navarro, A. B.; Putnis, A. Influence of chemical and structural factors on the calcite-calcium oxalate transformation. *CrystEngComm* **2013**, *15*, 9968−9979.

(22) Ruiz-Agudo, E.; Kudlacz, K.; Putnis, C. V.; Putnis, A.; Rodriguez-Navarro, C. Dissolution and carbonation of portlandite [$Ca(OH)_2$] single crystals. *Environ. Sci. Technol.* **2013**, *47*, 11342−11349.

DOI: 10.1021/acs.cgd.6b00522
Cryst. Growth Des. 2016, 16, 4950−4959

(23) Van Driessche, A. E. S.; Benning, L. G.; Rodriguez-Blanco, J. D.; Ossorio, M.; Bots, P.; Garcia-Ruiz, J. M. The Role and Implications of Bassanite as a Stable Precursor Phase to Gypsum Precipitation. *Science* **2012**, *336*, 69−72.
(24) Zhang, H.; De Yoreo, J. J.; Banfield, J. F. A Unified Description of Attachment-Based Crystal Growth. *ACS Nano* **2014**, *8*, 6526−6530.
(25) Imada, H.; Kimura, K.; Onishi, H. Water and 2-Propanol Structured on Calcite (104) Probed by Frequency-Modulation Atomic Force Microscopy. *Langmuir* **2013**, *29*, 10744−10751.
(26) Spagnoli, D.; Gilbert, B.; Waychunas, G. A.; Banfield, J. F. Prediction of the effects of size and morphology on the structure of water around hematite nanoparticles. *Geochim. Cosmochim. Acta* **2009**, *73*, 4023−4033.
(27) Rodríguez-Navarro, C.; Burgos-Cara, A.; Elert, K.; Putnis, C. V.; Ruiz-Agudo, E. Direct nanoscale imaging reveals the growth of calcite crystals via amorphous nanoparticles. *Cryst. Growth Des.* **2016**, *16*, 1850.
(28) Rubbo, M.; Bruno, M.; Massaro, F. R.; Aquilano, D. The five twin laws of gypsum (CaSO4 · 2 H2O): A theoretical comparison among the contact twin interfaces. *Cryst. Growth Des.* **2012**, *12*, 264−270.
(29) Pinto, A. J.; Jimenez, A.; Prieto, M. Interaction between phosphate-bearing solutions with gypsum: Epitaxy and induced twinning of brushite ($CaHPO_4{\cdot}2H_2O$) on the gypsum cleavage surface. *Am. Mineral.* **2009**, *94*, 313−322.
(30) Pinto, A. J.; Ruiz Agudo, E.; Putnis, C. V.; Putnis, A.; Jiménez, A.; Prieto, M. AFM study of the epitaxial growth of brushite ($CaHPO_4{*}2H_2O$) on gypsum cleavage surfaces. *Am. Mineral.* **2010**, *95*, 1747−1757.
(31) Alvarez-Lloret, P.; Rodríguez-Navarro, A.; Falini, G.; Fermani, S.; Ortega-Huertas, M. Crystallographic control on the hydrothermal conversion of calcitic sea Urchin Spine (Paracentrotus lividus) into apatite. *Cryst. Growth Des.* **2010**, *10*, 5227−5232.
(32) Morales, J.; Astilleros, J. M.; Fernández-Díaz, L.; Álvarez-Lloret, P.; Jiménez, A. Anglesite ($PbSO_4$) epitactic overgrowths and substrate-induced twinning on anhydrite ($CaSO_4$) cleavage surfaces. *J. Cryst. Growth* **2013**, *380*, 130−137.

DOI: 10.1021/acs.cgd.6b00522
Cryst. Growth Des. 2016, 16, 4950−4959